Colloid Polym Sci (2015) 293:239–248
DOI 10.1007/s00396-014-3402-x

ORIGINAL CONTRIBUTION

Self-assembly of star-shaped poly(2-isopropyl-2-oxazoline) in aqueous solutions

Alina I. Amirova · Marina M. Dudkina · Andrey V. Tenkovtsev · Alexander P. Filippov

Received: 28 July 2014 / Revised: 27 August 2014 / Accepted: 16 September 2014 / Published online: 8 October 2014

Abstract Eight-arm star-shaped poly(2-isopropyl-2-oxazoline) (PiPrOx) with calix[8]arene core ($M\approx$ 20,000 g mol^{-1}) was studied by turbidimetry and light scattering in aqueous solutions within concentration c ranging from 0.002 to 0.19 g cm^{-3}. The lower critical solution temperature (LCST) for PiPrOx is about 10 °C lower than for the linear analog. PiPrOx forms two types of particles at room temperature. The specie responsible for the fast mode is single macromolecules or 2–3 ones joined in aggregate with a hydrodynamic radius of 4.9 nm, irrespective of concentration. On heating, at first, growth of a large aggregate fraction was observed without variation of their hydrodynamic radii $R_h^{(s)}$. Then, $R_h^{(s)}$ increased up to 800 nm at c= 0.002 g cm^{-3}, while the fast mode disappeared. At all concentrations, the third middle mode with a size ranging from 9 to 40 nm was registered. It was observed in a very narrow temperature interval near the cloud point. The hydrodynamic radii of species and their fraction in solution were monitored as a function of time after the change in temperature.

Keywords Thermosensitive polymer · Star-shaped macromolecules · Static and dynamic light scattering · Lower critical solution temperature · Aggregation

Electronic supplementary material The online version of this article (doi:10.1007/s00396-014-3402-x) contains supplementary material, which is available to authorized users.

A. I. Amirova (✉) · M. M. Dudkina · A. V. Tenkovtsev · A. P. Filippov
Institute of Macromolecular Compounds, Russian Academy of Sciences, Bolshoy pr., 31, Saint Petersburg 199004, Russia
e-mail: aliram.new@gmail.com

Introduction

During the recent years, stimuli-responsive polymers have become ever more interesting objects for study due to the wide range of applications and ways for their modification [1, 2]. Within this class, thermosensitive polymers are probably the most investigated and widespread in our life as sensors, rheological additives, and multiple biological applications [3–5].

Special attention is given to star-shaped polymers [6, 7], which is due to a variety of means of changing their macromolecule structure and, consequently, polymer material properties. At present, stars with both low and high molecular weight core are synthesized, with the number, length, and composition of arms controlled [7].

Several aspects in the area of thermoresponsive star polymer in aqueous media are interesting to study. Solution transmittance measurement seems to be the first step that allows us to analyze some details of the thermosensitive star behavior. So, the role of the hydrophobic-hydrophilic balance, number, and a density of OH–groups in the thermosensitivity of polyglycidol stars with hydrophobic dendritic poly(tert-butyl-glycidylether) core is being investigated [8]. The authors have established the dependence of hydrodynamic dimensions of aggregate on sample composition and temperature T and estimated the aggregation number. F. Xu synthesized poly(N-isopropylacrylamide) star block copolymers with polylactide as a core and determined very low critical micelle concentration and the cloud point temperature (T_{cp}) at different pH [9]. The reversible phase changes in transmittance with T and the effect of the composition or the hydrophilic-hydrophobic chain length have been discussed.

Some scientific groups use dynamic light scattering (DLS) to observe the changes in solution properties of single macromolecules and the formed aggregates depending on T. For example, the effect of cyclodextrin end groups on the behavior

of star-shaped poly(N-isopropylacrylamide) with cyclodextrin core was analyzed [10]. While star macromolecules with cyclodextrin end groups and without them were characterized by close hydrodynamic radii R_h at room temperature, different temperature dependences of R_h were obtained. On heating, poly(N-isopropylacrylamide) star macromolecules formed micron-sized particles and precipitated, but the aggregates of macromolecules with hydrophilic cyclodextrin end groups did not exceed 50 nm. Moreover, the authors revealed reversibility of R_h values of aggregates upon cooling.

A. Dworak analyzed the role of composition and length of poly[di(ethylene glycol) methyl ether methacrylate-ran-oligo(ethylene glycol) methyl ether methacrylate] arms in temperature behavior of stars with hyperbranched poly(arylene oxindole) core [11]. Isolated star macromolecules were fixed at room temperature in water solutions. Above phase transition temperature, the character of concentration dependencies of R_h was different. Thus, the increase of arm length caused the steady growth of R_h values up to 1 μm with growing concentration. Also, the shape factor was measured at temperature below T_{cp} and above T_{cp} and the drop of shape factor was observed. Besides, its increase from 1 to 1.2 for aggregates with arm lengthening was reported.

It is obvious that polymers of different chemical classes are interesting as thermosensitive systems. In recent years, research into such isomers of well-studied polyacrylamides as poly(2-alkyl-2-oxazoline)s has been developing. They are promising as bio- and antimicrobial materials, thermoresponsive hydrogels and materials, in drug delivery, and in adhesive and coating formulations [12, 13]. The wide range of applications mentioned above, along with the advantages of star-shaped architecture of thermosensitive polymers have caused the intensive investigations of the behavior of star poly(2-alkyl-2-oxazoline)s.

Y. Chujo reported the synthesis, as well as DSC and TGA analysis of 4- or 5-arm poly(2-methyl-2-oxazoline) star on octafunctional silsesquioxane core [14]. Several works by Jin are devoted to poly(oxazoline) stars with porphyrin center and 4 arms. He studied the influence of the fabrication method on the size of micelles of poly(phenyloxazoline-block-methyloxazoline) in water/DMF mixtures [15] and suggested a procedure for assembly of (co)poly(2-alkyl-2-oxazoline)s star in water/chloroform emulsion [16]. Besides, self-organization of poly(phenyloxazoline-block-methyloxazoline) star was observed when sphere aggregates became network-like aggregates and formed a vesicular tube after 3-week aging [17].

There seems to be only one work which aims at studying the dependence of the properties of star-shaped poly(oxazoline) on T [18]. In particular, two series of poly(2-ethyl-2-oxazoline) stars with 6 or 13 arms and the length from 44 to 170 were investigated by UV-visible (UV-Vis) spectroscopy. For all samples, T_{cp} was 10÷20 °C lower than for linear poly(2-ethyl-2-oxazoline). Furthermore, T_{cp} went down from 75 to 62 °C with arm lengthening and the decrease in their number.

In our previous work, we investigated a water solution of the star-shaped poly(2-isopropyl-2-oxazoline) (PiPrOx) with eight arms and hydrophobic calix[8]arene core using methods of static and dynamic light scattering [19]. For the first time, both the temperature dependencies of scattered light intensity and hydrodynamic radii of scattering objects were obtained. We analyzed the time of reaching the equilibrium state of light intensity, and aggregate dimension values. In addition, three types of particles were fixed in solution of given concentration and the temperature range in which they were available was discussed. In order to develop this work further, we repeated the described procedures for solutions of other concentrations and can now report a detailed picture of PiPrOx thermosensitive star behavior in solution at varied temperature and concentration.

Experimental section

Synthesis and characterization of PiPrOx

The sample of star-shaped PiPrOx (Scheme 1) was prepared according to the procedure described previously [20]. The PiPrOx sample was synthesized as follows: the feeding monomer/initiator ratio was 1:20, the solvent was CH_3NO_2, the temperature was 70 °C, and the time of polymerization was 120 h. The polydispersity index of the arms (after hydrolysis) was 1.41 vs polyethylene oxide standards according to gel permeation chromatography data.

The molecular weight and hydrodynamic characteristics of PiPrOx under investigation were determined in the chloroform solution by static and dynamic light scattering, sedimentation-diffusion analysis, and viscometry [19]. The light scattering experiments resulted in the following values: weight-average molar mass M_w=19,600 g mol^{-1} and

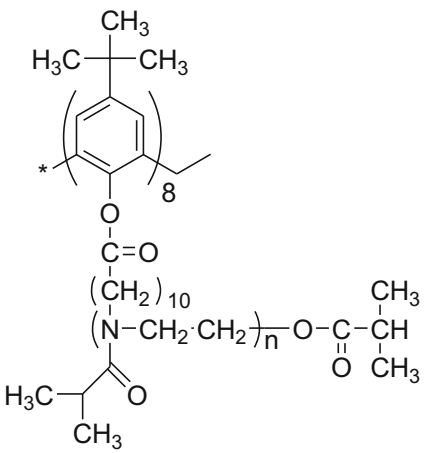

Scheme 1 Structure of star-shaped PiPrOx

hydrodynamic radius of macromolecules R_h=4.4 nm. The value of the so-called sedimentation-diffusion molar mass M_{sD}=22,100 g mol^{-1} was close to M_w. The viscometric hydrodynamic radius $R_{h\text{-}[\eta]}$ equal to 3.1 and 3.3 nm was calculated by Einstein equation using the intrinsic viscosity [η]= 9.8 cm^3 g^{-1} and the M_w or M_{sD} values, correspondingly. Note that the difference in the R_h and $R_{h\text{-}[\eta]}$ values is quite often observed for polymers with complex architecture [21–23] and is related to the fact that the equivalence principle for the radii of macromolecules does not hold during translational (diffusion) and rotational (intrinsic viscosity) motion [24].

Turbidimetry

Turbidity measurements were carried out on Cary 3 UV-Vis spectrophotometer (Varian, USA). The cloud point was determined by spectrophotometric detection of the changes in transmittance at λ=625 nm of the aqueous polymer solutions at concentration c=0.0050, 0.0100, 0.0200, 0.040, 0.050, 0.090, 0.120, 0.150, 0.170, and 0.190 g cm^{-3}. The solution temperature was increased at the rate of 0.1 grad min^{-1}. Given values for the cloud point were determined as the temperature corresponding to a 50 % decrease in optical transmittance.

Investigation of PiPrOx star behavior in aqueous solutions

The self-assembly of PiPrOx molecules near lower critical solution temperature (LCST) was studied by static and dynamic light scattering using Photocor Complex instrument (Photocor Instruments Inc., Russia) equipped with the Spectra-Physics He-Ne laser (wavelength λ=632.8 nm) as the light source. The correlation function of the scattered light intensity was obtained using Photocor-FC correlator with 288 channels. The scattering angle was 90 °. In equilibrium conditions, when solution characteristics did not change with time, the angle dependences of light scattering intensity I and hydrodynamic radii R_h of the scattering particles were also analyzed. The diffusion character of each type of particles was verified from the dependence of inverse relaxation time $1/\tau$ on squared wave vector q^2 (see Supporting Information, Fig. 1S). Note that at all solution concentrations and temperatures, the R_h values do not depend on scattering angle. This fact makes it possible to assume that the scattering objects in the PiPrOx solution investigated have symmetric form [25].

We have investigated six concentrations of PiPrOx solution in bidistilled water in the range from 0.0021 to 0.0324 g cm^{-3} and within the temperature interval from 21 °C to T_{cp}+8 °C. The solution temperature T was changed discretely, with the steps ranging from 2÷4 °C at low temperatures (when solution characteristics did not change with T) to 0.5÷1 °C near the cloud point. The heating rate was about 2 °C min^{-1}. The temperature was regulated with the precision of 0.1 °C.

After achieving the target T, we measured the light scattering intensity. If the rate of intensity change was too high, the dependence of I value on time t was analyzed only. At each temperature, we assumed that t=0 was the moment when the sample reached the required temperature. The hydrodynamic radius R_h of dissolved particles was measured when the intensity changed very weakly or independent of t. It should be noted that the values of R_h can be obtained correctly if the light scattering intensity differs no more than 1 % from its average value. The analysis of the dependences of I vs time in our experiments was within the range from 20 to 100 s. It is necessary to emphasize that the experiment time was equal to 1200 s at least at each temperature even if the measured characteristics did not depend on time.

In the cases when different scattering particles were present, the qualitative contribution of each particle type to the summary scattering intensity was estimated using the values of the square under the curved line of the corresponding I on R_h distribution peak.

All solutions were filtered into dust-free cells using Chromafil polyamide filters (Macherey-Nagel GmbH & Co. KG) with pore size of 0.20 μm.

Results and discussion

Determination of LCST

The temperature dependences of optical transmittance obtained for PiPrOx solution are typical for thermoresponsive polymers (inset in Fig. 1). At all concentrations, the temperature interval of transmittance change is narrow. Sharp solubility transitions are usually observed for linear poly(2-alkyl-2-oxazoline)s and may be explained by the fact that these polymers can only act as acceptors in hydrogen bonding [26].

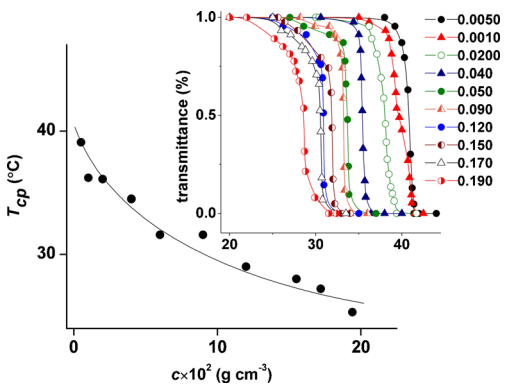

Fig. 1 Cloud point temperature T_{cp} vs concentration c. The *inset* shows dependences of relative transmittance of polymer solutions on T. The numbers near symbols are concentrations at which data were obtained

Figure 1 shows that T_{cp} decreases with the growth of solution concentration. However, no dependence minima are observed. So, unfortunately, it is impossible to determine exactly the LCST value but it is clear that LCST is lower or equal to 25 °C. Correspondingly, this temperature goes down by about 10 °C in comparison with linear PiPrOx with molecular weight 50,000 g mol^{-1} [27]. The data concerning LCST of linear PiPrOx with molecular weight similar to that of the star polymer under investigation is not available. We can compare the cloud points for linear and star polymers at c=0.02 g cm^{-3}. For linear PiPrOx with M=2500 g mol^{-1} [28], this is close to the molecular weight of the arm, T_{cp}=47 °C, while for the star investigated T_{cp}, equals to 37 °C. The influence of star-shaped architecture on phase transition temperature is probably due to its chemical nature and core size. It is clear that the massive hydrophobic core can cause the reduction of T_{cp}, as observed for PiPrOx investigated.

Temperature dependences of star-shaped PiPrOx solution characteristics

For all the investigated solutions, we registered similar qualitative behavior. Figures 2, 3, and 4 show the dependences of the light scattering intensity, hydrodynamic radii of scattering objects, and the ratio of squares under the peaks of intensity scattering curve on T for particular concentrations.

Bimodal distribution of intensity I on the hydrodynamic radius of scattering particles was observed even at room temperature (see Fig. 5). The hydrodynamic radii of slow $R_h^{(s)}$ and fast $R_h^{(f)}$ modes differ considerably. On the other hand, the squares under the peak curves corresponding to slow $S^{(s)}$ and fast $S^{(f)}$ modes are close (Fig. 4): the $S^{(s)}/S^{(f)}$ values lie in the range from 0.6 to 1.6 for different concentrations. Correspondingly, given that I depend strongly on the scattering particle size, we may assume that small particles (fast mode) prevail in solution at room temperature. Indeed,

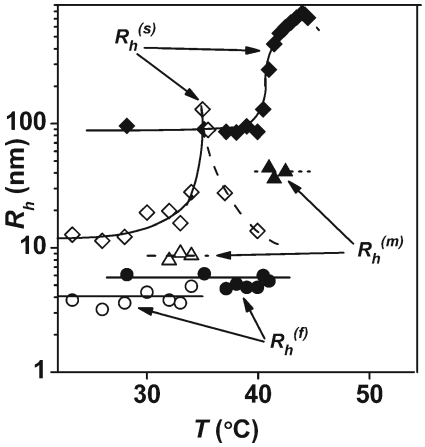

Fig. 3 Temperature dependences of hydrodynamic radii R_h of scattering species for PiPrOx solutions with c=0.0021 g cm^{-3} (*closed symbols*) and c=0.0324 g cm^{-3} (*open symbols*)

according to the static light scattering theory (see, for example, monographs [29, 30]), the intensity I_i of ith specie is proportional to both the molar mass M_i and concentration c_i of particles as follows from the simplified form of the Rayleigh equation $I_i \sim c_i M_i$. The particle radius R_i is related to its molar mass as $M_i \sim R_i^x$, where parameter x depends on the particle shape (x=3 for rigid sphere, 2 for macromolecular coil, and 1 for long rod). We can assume that the form of scattering objects in the investigated PiPrOx solutions is close to spherical; correspondingly, $x \approx 3$. Consequently, $I_i \sim c_i R_i^3$ and at fixed particle concentration $I_i \sim R_i^3$. Thus, rough estimation assuming spherical scattering objects shows that the fraction of the large aggregates at low temperatures does not exceed 0.05 at any concentration.

Note that D. Momekova et al. have also registered two modes at room temperature studying the star-shaped poly(ethylene oxide) with calix[4]arene core [31]. Moreover, they established the influence of the arm length on the species set in solution. The degree of polymerization of arm up to 26 resulted in the formation of two particle types in water

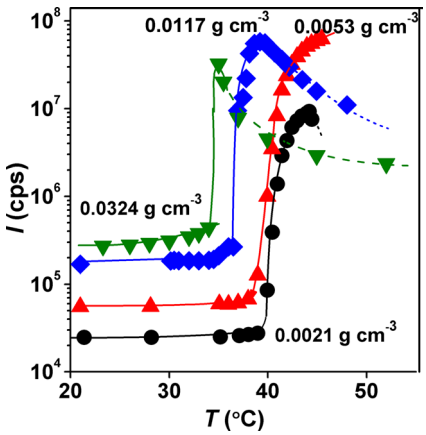

Fig. 2 Temperature dependences of apparent light scattering intensity for PiPrOx solutions

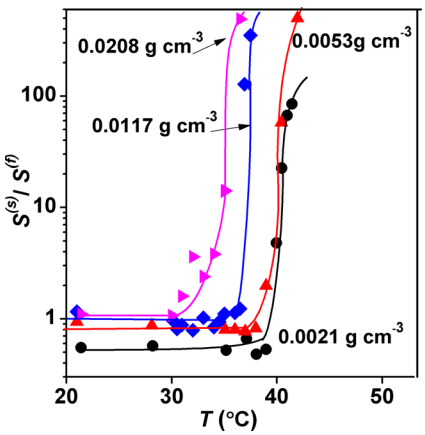

Fig. 4 Temperature dependences of $S^{(s)}/S^{(f)}$ ratio of squares under the peaks of slow and fast modes for PiPrOx solutions

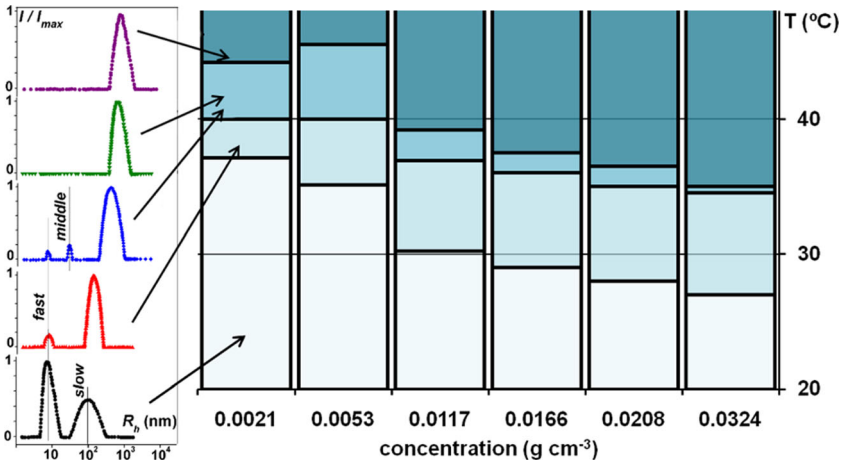

Fig. 5 The temperature diagram of PiPrOx solutions and the corresponding light scattering intensity distribution on hydrodynamic radius

solution, while high molecular weight stars formed uniform particles with R_h=(78÷122)nm. In the case of the PiPrOx sample investigated by us, the arm polymerization degree was close to 20.

Figures 2, 3, and 4 show that the characteristics of PiPrOx solutions do not depend on T at low temperatures. The I values begin to increase slightly at $T_{cp}-T>8$ °C (Fig. 2). The intensity change is not so large and reaches 2–7 % on 1 °C. This negligible growth of I occurs up to $T_{cp}-T=(0.5\div5.5)$°C. Within the considered temperature interval, the hydrodynamic radii $R_h^{(f)}$ and $R_h^{(s)}$ are independent of T (Fig. 3), whereas the $S^{(s)}/S^{(f)}$ ratio increases (Fig. 4). Correspondingly, elevation in the light scattering intensity can be explained by the change in composition of scattering objects. The fraction of large particles (slow mode) grows and the fraction of species responsible for the fast mode decreases.

At $T_{cp}-T<(0.5\div5.5)$°C the characteristics of PiPrOx solutions change dramatically (Figs. 2, 3, and 4): (i) the light scattering intensity increases 5÷20 times with heating of samples by 0.5 °C; (ii) the ratio $S^{(s)}/S^{(f)}$ of the squares under intensity distribution peaks grows strongly with the temperature increase and the fast mode vanishes (an increase in $S^{(s)}/S^{(f)}$ is accompanied by practically symbate change of the I value [19]); (iii) the rise of hydrodynamic radius $R_h^{(s)}$ of the slow mode is observed; and (iv) a new third mode appears.

What is really interesting is the appearance of this latter mode. Its hydrodynamic radius $R_h^{(m)}$ is smaller than $R_h^{(s)}$ but larger than $R_h^{(f)}$ (Fig. 4), thus we called it the "middle" mode [19]. The behavior of the middle mode varies for different concentrations. For solution at c=0.0117 g cm^{-3}, the middle-sized particles are not observed. At concentration c= 0.0166 g cm^{-3}, the middle mode arises after the disappearance of the fast mode. For the remaining concentrations, the three modes (slow, middle, and fast) co-exist simultaneously within a very narrow temperature range (<2 °C). The $R_h^{(m)}$ is constant at given concentration, but the fraction of middle-sized particles in solution decreases rapidly with the temperature growth, and the middle mode also disappears.

At $T_{cp}-T<(0.5\div3)$°C, we observed only the slow mode in PiPrOx solutions. Its radius $R_h^{(s)}$ increased with the temperature rise up to about 780 nm for the most diluted system. We obtained values of the same order of magnitude that were reported earlier for poly(N-isopropylacrylamide) star [10] and linear (co)poly(2-isoprosyl-2-oxazoline)s [32, 33] at $c\leq$ 0.001 g cm^{-3}. This behavior is typical for thermosensitive polymers of different chemical structure and architecture, in particular, for polyoxazolines.

The maximum values of scattering intensity and hydrodynamic radius $R_h^{(s)}$ are achieved at temperature T_{max}, which is close for majority of concentrations to the cloud point temperature T_{cp} determined by turbidimetry.

Above $T_{max}\approx T_{cp}$, I and $R_h^{(s)}$ values decrease with temperature rise (Fig. 2). However, the solutions were very turbid. We could not achieve transparency of solution even at T= 60 °C. Correspondingly, light scattering is not classical in this temperature interval. Therefore, the measured hydrodynamic radii are apparent and the quantitative analysis is impossible.

Summarizing the analysis of temperature dependences of star-shaped PiPrOx solution characteristics, we can conclude that the main phase transition mechanism in the system under study is the growth of very large aggregates. They collapse above cloud point, which is qualitatively confirmed by the observed reduction of hydrodynamic radii.

Concentration dependences of PiPrOx solution characteristics

As mentioned above, two types of species exist in PiPrOx solutions at room temperature. As seen from Table 1, the hydrodynamic radius $R_h^{(f)}$ corresponding to the fast mode does not depend on the concentration (Fig. 2S). The average value of $R_h^{(f)}$ (both for the temperature and the concentration) is equal to 4.9 nm. It is slightly larger than the hydrodynamic radii R_h and $R_{h\text{-}[\eta]}$ of isolated PiPrOx macromolecules obtained in chloroform solution [19]. Therefore, we can assume that the particles responsible for the fast mode are individual star-

Table 1 Temperature and hydrodynamic characteristics of PiPrOx solutions

c (g cm^{-3})	T_{start} (°C)	T_{rapid} (°C)	T_{max} (°C)	$T^{(s)\text{-}i}$ (°C)	$T^{(f)\text{-}d}$ (°C)	$T^{(m)\text{-}a}$ (°C)	$T^{(m)\text{-}d}$ (°C)	$R_h^{(f)a}$ (nm)	$R_h^{(m)a}$ (nm)	$R_h^{(s)b}$ (nm)	$R_h^{(s\text{-}max)}$ (nm)	$S^{(s)}/S^{(f)b}$
0.0021	37.1	40.0	44.2	40.5	41.4	41.0	42.5	5.2	40	90	780	0.6
0.0053	35.1	40.0	45.5	40.0	42.0	40.0	42.4	4.9	24	91	380	0.9
0.0117	30.2	36.9	39.2	37.8	37.8	–	–	5.5	–	53	75	0.9
0.0166	29.0	36.0	37.5	36.5	36.5	36.2	36.5	5.0	14	28	84	0.8
0.0208	28.0	35.0	36.5	35.0	36.0	35.5	36.0	4.6	13	21	86	1.1
0.0324	27.0	34.5	35.0	34.0	34.0	32.0	34.0	4.2	8.6	15	130	1.6

[a] Values average over all temperatures

[b] Obtained at room temperature

shaped macromolecules of PiPrOx or small aggregates (two or three macromolecules).

On the contrary, the hydrodynamic radius of the slow mode depends on the concentration. The $R_h^{(s)}$ value grows rapidly with the dilution rate (Table 1 and Fig. 2S). This change may be caused by the concentration dependence of the diffusion coefficient D_0 of large species or the increase of their size. We suppose that both factors could be the reason of the observed growth of $R_h^{(s)}$; however, it is impossible to distinguish the contribution of each.

It is possible that the nature of large particles detected in PiPrOx solutions is similar to that of the aggregates which are formed in an aqueous solutions of the linear poly(2-alkyl-2-oxazoline)s [32–35]. We estimated roughly the minimum of the aggregation number using the model of a rigid sphere for both star-shaped PiPrOx molecules and large particles. The value m of macromolecules in the aggregate is close to the ratio of volumes of the aggregate (V_{ag}) and the macromolecule (V_m). For spherical particles, the volume is proportional to third power of their radius and correspondingly $m \approx (R_h^{(s)}/R_h^{(f)})^3$. The minimum value of $R_h^{(s)}$ obtained at c= 0.0324 g cm^{-3} at room temperature is equal to 15 nm; consequently, the minimum aggregation number is $m \approx (15/4.9)^3 \approx 30$.

As regards to the formation of the particles responsible for the middle mode, the reason for this is not clear and the solution of this problem requires further research. The hydrodynamic radius $R_h^{(m)}$ of the middle species is practically constant in the concentration interval from 0.0117 to 0.0324 g cm^{-3}, but at low c, the $R_h^{(m)}$ increases with the decrease of solution concentration (Fig. 2S). The size of the middle mode is not large. In spherical particle approach, the minimum aggregation number was close to 10 at the maximum concentration of PiPrOx solution.

As described above, the hydrodynamic radius $R_h^{(s)}$ reached the maximum value $R_h^{(s\text{-}max)}$ near the cloud point temperature. Table 1 shows the concentration dependence of $R_h^{(s\text{-}max)}$ which is not monotonic (Fig. 3S). At concentrations higher than 0.0117 g cm^{-3}, the $R_h^{(s\text{-}max)}$ value increases from 75 to 130 nm with the growth of c. In the low concentration region, $R_h^{(s\text{-}max)}$ increases strongly with concentration decrease and reaches the maximum at c=0.0021 g cm^{-3}. The aggregation number m_{max} is very large at $T \rightarrow T_{max}$. For spherical particle model, the estimation of m_{max} gives about 4000 at c= 0.0117 g cm^{-3}. The hydrodynamic dimensions and aggregation number obtained are close to the data for block copolymers of PiPrOx and poly(2-ethyl-2-oxazoline) [35].

For all concentrations, we may single out three temperature regions below T_{max} (Fig. 5). At low T (first temperature interval), the PiPrOx solution is practically a solution of macromolecules or small aggregates with a low fraction of large particles. Notably, the composition of the solution varies significantly at room temperature. In particular, the higher the concentration, the higher the $S^{(s)}/S^{(f)}$ ratio, i.e., the fraction of large specie (Figure 4S). In the second region, only these two types of scattering objects exist in solution and their hydrodynamic radii $R_h^{(s)}$ and $R_h^{(f)}$ do not depend on the temperature either. Only an insignificant increase of the $S^{(s)}/S^{(f)}$ ratio is observed, i.e., the solution composition changes. The large aggregate fraction grows slowly and the corresponding increase of light scattering intensity is observed. The temperature T_{start}, at which the intensity change begins, decreases with c from 37 to 26 °C (Figs. 5 and 5S). At high concentrations, the width of the second temperature interval does not depend on c and is equal to (6.5÷7.5)°C. In the case of low concentration solution, this region narrows down to 5 °C (c= 0.0053 g cm^{-3}) and 3 °C (c=0.0021 g cm^{-3}).

The third temperature field established by light scattering methods (Fig. 5) practically coincides with the intervals of reduction of relative transmittance (Fig. 1). At given concentration, this region can be considered as phase transition. The discussed temperature interval $T_{max} - T_{rapid}$ is expended with concentration decrease from 0.5 °C at c=0.0324 g cm^{-3} to (4÷5.5)°C for more diluted solutions (Figs. 5 and 5S). T_{rapid} is temperature at which the rapid increase of light scattering intensity begins; this is the low boundary of the third temperature field (Table 1). As a result, the total width of the interval $T_{max} - T_{start}$, where the characteristic changes took place (the second and third region) increases slowly from 8 °C at

maximum concentration to 10.5 °C at c=0.0053 g cm^{-3}. However, $T_{max}-T_{start}$=7 °C at c=0.0021 g cm^{-3}.

The strong growth of scattering intensity I near T_{max} (in the third temperature interval) is caused by several factors. The first is the rapid change of the ratio of small and large particles in solutions (Fig. 4). The number of the latter increases due to the reduction of the number of macromolecules or small aggregates. Correspondingly, the average size of the scattering objects rises and so the significant change in the I value takes place. The redistribution of scattering objects with $R_h^{(f)}$ and $R_h^{(s)}$ occurs intensively and finishes with the disappearance of small species in solution at temperature $T^{(f)-d}$ (Table 1). At temperature $T^{(s)-i}$ (Table 1), a remarkable growth of the hydrodynamic radius of the slow mode begins. It is the second reason for the impetuous change of I. As seen from Table 1, both $T^{(f)-d}$ and $T^{(s)-i}$ decrease with the concentration increase (Fig. 6S). For the three concentrations, the expansion of large aggregates begins before the fast mode disappearance and $T^{(f)-d}-T^{(s)-i}<2$ °C. On the other hand, $T^{(f)-d}=T^{(s)-i}$ at c=0.0117, 0.0166, and 0.0324 g cm^{-3}.

In the third temperature interval, we established the middle mode, whose appearance $T^{(m)-a}$ and disappearance $T^{(m)-d}$ temperatures decrease with concentration growth (Table 1 and Fig. 7S). The interval $T^{(m)-d}-T^{(m)-a}$ of the middle mode presence is very narrow. It is minimum (0.3 °C) for the solution with c=0.0166 g cm^{-3} and maximum (2.4 °C) for c= 0.0053 g cm^{-3}. Under these temperatures, the particle redistribution occurs: the fraction of the middle-sized particles decreases and number of the large aggregates grows. Note that the presence of more than two modes in the solution of thermosensitive polymers was also established by other groups. For example, three particle types were observed for water-soluble conjugates of poly(ethylene glycol) [36] and miktoarm stars [37]. The latter formed unimers, micellar-like structures, and loose aggregates in solutions, as the authors called these objects. It could be assumed that the reported unimers and loose aggregates correspond to small and large aggregates observed by us in the PiPrOx star solution investigated. Their dimensions are comparable and the temperature below phase transition is the same for both systems. The hydrodynamic radii of the PiPrOx middle mode and the miktoarm star micellar-like structures are also close. However, these objects display a very different behavior. Miktoarm star micellar-like structures are stable. They exist in all temperature intervals investigated and disappear near cloud point. The main feature of the PiPrOx middle mode is that it occurs within a rather narrow interval (0.3÷2)°C appearing and disappearing near T_{max}. Probably, they are unstable and cannot be formed at relatively low temperatures.

Figure 5 and Table 1 illustrate the dependences of T_{max}, and correspondingly cloud point temperature at solution concentration c. As one would expect, the T_{cp} and T_{max} values decrease with concentration growth. Such behavior is typical for thermoresponsive polymers with different architecture, namely, the linear, star-shaped, and grafted systems [13, 27, 38].

Time dependences of PiPrOx solution characteristics

All measured characteristics of the PiPrOx solutions change very slowly after the temperature is changed. This fact is illustrated in Figs. 6 and 7, which show the time dependences of scattering intensity, hydrodynamic radius, and the $S^{(s)}/S^{(f)}$. We do not analyze these changes quantitatively because it is a complicated problem and can be the purpose of a future study. We will try to describe the kinetics on the qualitative level.

All time dependences of intensity for PiPrOx solutions have S-shaped form. After reaching a certain temperature, the I value does not change or grows very slightly (Fig. 6). The duration of this period is 100–200 s and does not depend on the temperature and concentration. After that, a more or less rapid increase of light scattering intensity is observed. The equilibrium value of scattering intensity reaches at time t_{eq}. For the low concentration solutions ($c\leq$0.0053 g cm^{-3}), this time is practically independent of the temperature and t_{eq} is smaller than 3000 s. Almost similar value of t_{eq} is observed for more concentrated solution at rather low temperatures (Fig. 6). The time necessary for equilibrium achievement grows significantly with heating the solution; near T_{cp} (in the third temperature interval) the t_{eq} value may exceed 40,000 s.

It is impossible to establish the change of $R_h^{(s)}$ and $S^{(s)}/S^{(f)}$ when the intensity increases rapidly. Therefore, we obtained broken dependences of these characteristics on time (Fig. 7): we measured the $R_h^{(s)}$ and $S^{(s)}/S^{(f)}$ values at small t<200 s and at large t when the scattering intensity changed slightly. However, we can conclude that the discussed parameters grow with t, causing the increase of I value. Note that the change of the middle mode fraction with time is similar to the dependence of $S^{(s)}/S^{(f)}$ on t.

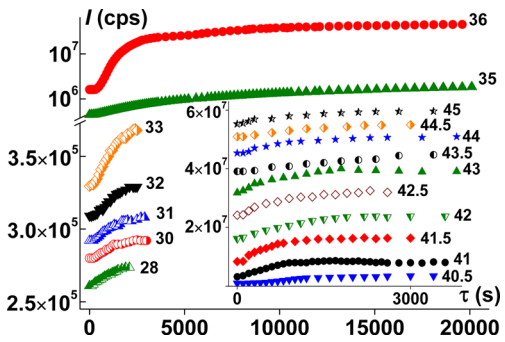

Fig. 6 Time dependences of relative intensity I/I_0 for c=0.0324 and c= 0.0053 g cm^{-3} (*inset*). I_0 is the light scattering intensity at t=0 for given temperature. The numbers near dependences are temperatures at which data were obtained

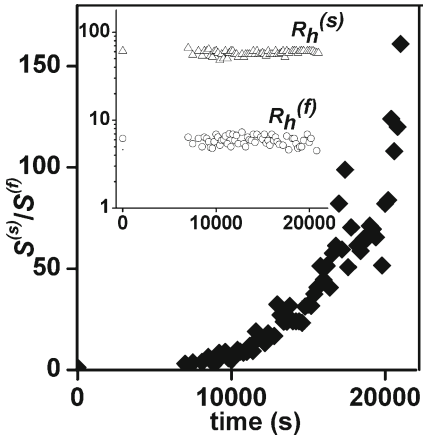

Fig. 7 Time dependence of hydrodynamic radii of slow $R_h^{(s)}$ and fast $R_h^{(f)}$ modes and the ratio of the squares under corresponding curves $S^{(s)}/S^{(f)}$ for solution of c=0.0117 g cm^{-3} at T=37 °C

As far as we know, nobody has yet reported such prolonged processes of system stable state achievement. As a rule, the solvents are retained for a time period from 3 min to 1 h before the light scattering experiment are performed [39–42], and the time dependence of intensity is not observed. Time evolution of solvent characteristics was established for linear block copolymers of poly(2-isopropyl-2-oxazoline) with poly(2-ethyl-2-oxazoline) [35]. However, the experiment duration did not exceed 40 min. Important quantitative information about the aggregation rate was obtained for thermosensitive massive (radius is 30–50 nm) polystyrene/poly(N-isopropylacrylamide) core-shell nanoparticles [43]. The combination of theoretical kinetic model of the association/dissociation with the analysis of dynamic light scattering data showed that the binding energy changes sharply with temperature. The investigated time interval was 800 s, but the authors pointed out that at high temperatures the duration of the hydrodynamic radius evolution of colloidal suspension increases remarkably.

At this point, the question logically arises: why was the very large t_{eq} not observed previously? We can make the following assumptions. Firstly, in the overwhelming majority of works, only very low-concentrated solutions ($c\leq$ 0.001 g cm^{-3}) are investigated using light scattering methods [11, 35, 37, 39, 41, 44]. As shown above, the duration of equilibrium achievement depends strongly on concentration, and for PiPrOx solutions, t_{eq}<3500 s at $c\leq$0.005 g cm^{-3} (Fig. 6). It could be suggested that at $c\leq$0.001 g cm^{-3}, this time will be even less, and hence, it is impossible to register the kinetics of the changes due to the conditions of the experiment. Secondly, the star-shaped architecture of PiPrOx macromolecules investigated should be taken into account. The density of star macromolecules is higher than the corresponding parameter for isolated linear polymer molecules or micelles. The hydrophilic shell prevents the contacts and weakens interaction between the hydrophobic fragments of different macromolecules or their aggregates. As a result, the growth of large aggregates slows down sharply. And finally, we should keep in mind that the prolonged processes of equilibrium achievement are observed in the narrow temperature interval (0.5÷2.0 °C) near cloud point.

Conclusion

LCST of star-shaped PiPrOx does not exceed 25 °C, which is close to LCST found for PiPrOx with a different architecture. Unfortunately, it is impossible to determine the influence of star structure on LCST because of the difference in M of our sample and PiPrOx studied by other scientific groups.

It was found that in the interval of concentrations under investigation, the star-shaped PiPrOx polymer in aqueous solutions forms two types of particles even at room temperature. The size of the small species does not depend on c. The objects responsible for the fast mode are single macromolecules or two or three ones joined in an aggregate. Note also that the fraction of these aggregates in solution decreases slightly with concentration increase. The hydrodynamic radius of the large particles grows both with temperature and concentration increase.

On heating, the polymer solution characteristics change. This transition is not jump-like and occurs within the temperature interval of (6÷10)°C, the width of which does not depend on solution concentration. At the first stage of this range, the redistribution of scattering objects begins due to the increase of large component fraction without variation of the hydrodynamic radii of the scattering objects. Consequently, slow increase in light scattering intensity is observed. Then, the growth intensity accelerates. This is caused by several changes occurring in PiPrOx solutions. The $S^{(s)}/S^{(f)}$ increase becomes very intensive and the small species disappear. Besides, the rise of large particle size takes place. Moreover, a new middle-sized mode arises. Its hydrodynamic dimensions are constant at a given concentration. Notably, the particles responsible for this mode exist in a narrow temperature interval (0.3÷2)°C near T_{max}. Finally, only large particles remain in the solution, and $R_h^{(s)}$ increases and reaches the maximum at cloud point. Above T_{cp}, we established only one mode, whose apparent dimensions go down with the increase of T.

It is interesting to point out that the achievement of the equilibrium state after the transition from one temperature to another requires an unexpectedly long time. For the low-concentration solutions, this time is practically independent of the temperature and does not exceed 3000 s. For high-concentrated solutions, similar values are detected at low temperatures. However, the duration of equilibrium achievement grows significantly with solution heating.

Acknowledgments The financial support was given by the Russian Science Foundation (project no. 14-13-00231).

References

1. Liu F, Urban MW (2010) Recent advances and challenges in designing stimuli-responsive polymers. Prog Polym Sci 35:3–23. doi:10.1016/j.progpolymsci.2009.10.002
2. Theato P, Sumerlin BS, O'Reilly RK, Epps TH III (2013) Stimuli responsive materials. Chem Soc Rev 42:7055–7056. doi:10.1039/C3CS90057F
3. Liu R, Fraylich M, Saunders BR (2009) Thermoresponsive copolymers: from fundamental studies to applications. Colloid Polym Sci 287:627–643. doi:10.1007/s00396-009-2028-x
4. Ward MA, Georgiou TK (2011) Thermoresponsive polymers for biomedical applications. Polymers 3:1215–1242. doi:10.3390/polym3031215
5. Jochum FD, Theato P (2013) Temperature- and light-responsive smart polymer materials. Chem Soc Rev 42:7468–7483. doi:10.1039/C2CS35191A
6. Iatridi Z, Tsitsilianis C (2011) Water-soluble stimuli responsive star-shaped segmented macromolecules. Polymers 3:1911–1933. doi:10.3390/polym3041911
7. Kuckling D, Wycisk A (2013) Stimuli-responsive star polymers. J Polym Sci Part A: Polym Chem 51:2980–2994. doi:10.1002/pola.26696
8. Libera M, Walach W, Trzebicka B, Rangelov S, Dworak A (2011) Thermosensitive dendritic stars of tert-butyl-glycidylether and glycidol—synthesis and encapsulation properties. Polymer 52:3526–3536. doi:10.1016/j.polymer.2011.06.003
9. Xu F, Zheng SZ, Luo YL (2013) Thermosensitive t-PLA-b-PNIPAAm tri-armed star block copolymer nanoscale micelles for camptothecin drug release. J Polym Sci Part A: Polym Chem 51:4429–4439. doi:10.1002/pola.26859
10. Liu YY, Zhong YB, Nan JK, Tian W (2010) Star polymers with both temperature sensitivity and inclusion functionalities. Macromolecules 43:10221–10230. doi:10.1021/ma1019973
11. Kowalczuk A, Mendrek B, Zymelka-Miara I, Libera M, Marcinkowski A, Trzebicka B, Smet M, Dworak A (2012) Solution behavior of star polymers with oligo(ethylene glycol) methyl ether methacrylate arms. Polymer 53:5619–5631. doi:10.1016/j.polymer.2012.10.022
12. Schlaad H, Diehl C, Gress A, Meyer M, Demirel AL, Nur Y, Bertin A (2010) Poly(2-oxazoline)s as smart bioinspired polymers. Macromol Rapid Commun 31:511–525. doi:10.1002/marc.200900683
13. Weber C, Hoogenboom R, Schubert US (2012) Temperature responsive bio-compatible polymers based on poly(ethylene oxide) and poly(2-oxazoline)s. Prog Polym Sci 37:686–714. doi:10.1016/j.progpolymsci.2011.10.002
14. Kim KM, Ouchi Y, Chujo Y (2003) Synthesis of organic-inorganic star-shaped polyoxazolines using octafunctional silsesquioxane as an initiator. Polym Bull 49:341–348. doi:10.1007/s00289-002-0113-0
15. Jin RH (2002) Controlled location of porphyrin in aqueous micelles self-assembled from porphyrin centered amphiphilic star poly(oxazolines). Adv Mater 14:889–892. doi:10.1002/1521-4095(20020618)14:12<889::AID-ADMA889>3.0.CO;2-6
16. Jin RH (2004) Water soluble star block poly(oxazoline) with porphyrin label: a unique emulsion and its shape direction. J Mater Chem 14:320–327. doi:10.1039/B307439K
17. Jin RH (2003) Self-assembly of porphyrin-centered amphiphilic star block copolymer into polymeric vesicular aggregates. Macromol Chem Phys 204:403–409. doi:10.1002/macp.200390008
18. Kowalczuk A, Kronek J, Bosowska K, Trzebicka B, Dworak A (2011) Star poly(2-ethyl-2-oxazoline)s—synthesis and thermosensitivity. Polym Int 60:1001–1009. doi:10.1002/pi.3103
19. Filippov AP, Amirova AI, Dudkina MM, Tenkovtsev AV (2013) Thermoresponsive star-shaped poly(2-isopropyl-2-oxazoline) in aqueous solution. Int J Polym Anal Charact 18:567–577. doi:10.1080/1023666X.2013.836925
20. Ten'kovtsev AV, Trofimov AE, Shcherbinskaya LI (2012) Thermoresponsive star-shaped poly(2-isopropyl-2-oxazolines) based on octa-tert-butylcalix[8]arene. Polym Sci B 54:142–148. doi:10.1134/S1560090412030098
21. Filippov AP, Romanova OA, Vinogradova LV (2010) Molecular and hydrodynamic characteristics of star-shaped polystyrenes with one or two fullerene (C60) molecules as a branching center. Polym Sci A 52:221–227. doi:10.1134/S0965545X10030016
22. Filippov AP, Belyaeva EV, Tarabukina EB, Amirova AI (2011) Behavior of hyperbranched polymers in solutions. Polym Sci C 53:107–117. doi:10.1134/S1811238211060014
23. Filippov AP, Zamyshlyayeva OG, Tarabukina EB, Simonova MA, Kozlov AV, Semchikov YD (2012) Structural and conformational properties of hyperbranched copolymers based on perfluorinated germanium hydrides. Polym Sci A 54:319–329. doi:10.1134/S0965545X12050033
24. Tsvetkov VN (1989) Rigid-chain polymers. Plenum, New York
25. Berne BJ, Pecora R (2000) Dynamic light scattering with applications to chemistry, biology, and physics. Wiley, New York
26. Salzinger S, Huber S, Jaksch S, Busch P, Jordan R, Papadakis CM (2012) Aggregation behavior of thermo-responsive poly(2-oxazoline)s at the cloud point investigated by FCS and SANS. Colloid Polym Sci 290:385–400. doi:10.1007/s00396-011-2564-z
27. Aseyev V, Tenhu H, Winnik FM (2011) Non-ionic thermoresponsive polymers in water. Adv Polym Sci 242:29–89. doi:10.1007/12_2010_57
28. Huber S, Jordan R (2008) Modulation of the lower critical solution temperature of 2-alkyl-2-oxazoline copolymers. Colloid Polym Sci 286:395–402. doi:10.1007/s00396-007-1781-y
29. Kratochvil P (1987) Classical light scattering from polymer solution. Elsevier, Amsterdam
30. Schärtl W (2007) Light scattering from polymer solutions and nanoparticle dispersions. Springer, Berlin
31. Momekova D, Budurova D, Drakalska E, Shenkov S, Momekov G, Trzebicka B, Lambov N, Tashev E, Rangelov S (2012) Aggregation behavior and in vitro biocompatibility study of octopus-shaped macromolecules based on tert-butylcalix[4]arenes. Int J Pharm 436:410–417. doi:10.1016/j.ijpharm.2012.06.053
32. Obeid R, Maltseva E, Thünemann AF, Tanaka F, Winnik FM (2009) Temperature response of self-assembled micelles of telechelic hydrophobically modified poly(2-alkyl-2-oxazoline)s in water. Macromolecules 42:2204–2214. doi:10.1021/ma802592f
33. Hruby M, Filippov SK, Panek J, Novakova M, Mackova H, Kucka J, Ulbrich K (2010) Polyoxazoline thermoresponsive micelles as radionuclide delivery systems. Macromol Biosci 10:916–924. doi:10.1002/mabi.201000034
34. Caponi PF, Qiu XP, Vilela F, Winnik FM, Ulijn RV (2011) Phosphatase/temperature responsive poly(2-isopropyl-2-oxazoline). Polym Chem 2:306–308. doi:10.1039/C0PY00291G
35. Takahashi R, Sato T, Terao K, Qiu XP, Winnik FM (2012) Self-association of a thermosensitive poly(alkyl-2-oxazoline) block copolymer in aqueous solution. Macromolecules 45:6111–6119. doi:10.1021/ma300969w
36. Domnina NS, Sergeeva OY, Koroleva AN, Rakitina OV, Dobrun LA, Filippov SK, Mikhailova ME, Lezov AV (2010) Molecular properties of conjugates formed by synthetic hydrophilic polymers and sterically hindered phenols. Polym Sci A 52:900–906. doi:10.1134/S0965545X1009004X

37. Steinschulte AA, Schulte B, Rütten S, Eckert T, Okuda J, Möller M, Schneider S, Borisov OV, Plamper FA (2014) Effects of architecture on the stability of thermosensitive unimolecular micelles. Phys Chem Chem Phys 16:4917–4932. doi:10.1039/c3cp54707h
38. Roy D, Brooks WLA, Sumerlin BS (2013) New directions in thermoresponsive polymers. Chem Soc Rev 42:7214–7243. doi:10.1039/C3CS35499G
39. Han X, Zhang X, Zhu H, Yin Q, Liu HL, Hu Y (2013) Effect of composition of PDMAEMA-b-PAA block copolymers on their pH- and temperature-responsive behaviors. Langmuir 29:1024–1034. doi:10.1021/la3036874
40. Meyer M, Antonietti M, Schlaad H (2007) Unexpected thermal characteristics of aqueous solutions of poly(2-isopropyl-2-oxazoline). Soft Matter 3:430–431. doi:10.1039/B616678D
41. Bühler J, Muth S, Fischer K, Schmidt M (2013) Collapse of cylindrical brushes with 2-isopropyloxazoline side chains close to the phase boundary. Macromol Rapid Commun 34:588–594. doi:10.1002/marc.201200784
42. Korchagina EV, Qiu XP, Winnik FM (2013) Effect of heating rate on the pathway for vesicle formation in salt-free aqueous solutions of thermosensitive cationic diblock copolymers. Macromolecules 46:2341–2351. doi:10.1021/ma302666e
43. Zaccone A, Crassous JJ, Béri B, Ballauff M (2011) Quantifying the reversible association of thermosensitive nanoparticles. Phys Rev Lett 107:168303(4). doi:10.1103/PhysRevLett.107.168303
44. Xu Y, Bolisetty S, Drechsler M, Fang B, Yuan J, Ballauff M, Müller AHE (2008) pH and salt responsive poly(N, N-dimethylaminoethyl methacrylate) cylindrical brushes and their quaternized derivatives. Polymer 49:3957–3964. doi:10.1016/j.polymer.2008.06.051